Available online at www.sciencedirect.com
SCIENCE DIRECT
Journal of Molecular Catalysis A: Chemical 247 (2006) 171–181
JOURNAL OF MOLECULAR CATALYSIS A: CHEMICAL
www.elsevier.com/locate/molcata

Catalytic nitroxidation of 1-methylnaphthalene I. Preparation, characterisation and NO-surface interactions of chromia/alumina-based catalysts

E. Rombi [a], M.G. Cutrufello [a], S. De Rossi [b], M.F. Sini [a], I. Ferino [a,*]

[a] *Università di Cagliari, Dipartimento di Scienze Chimiche, Complesso Universitario Monserrato, s.s. 554 Bivio Sestu, 09042 Monserrato (CA), Italy*
[b] *Istituto dei Sistemi Complessi (ISC) del CNR, Sezione "Materiali Inorganici e Catalisi Eterogenea" (MICE), c/o Dipartimento di Chimica, Università di Roma "La Sapienza", Piazzale Aldo Moro 5, 00185 Roma, Italy*

Received 24 October 2005; received in revised form 21 November 2005; accepted 23 November 2005
Available online 18 January 2006

Abstract

In view of their use in the nitroxidation of 1-methylnaphthalene into 1-naphthonitrile, chromia/alumina and K-containing chromia/alumina catalysts were prepared. They were characterised by X-ray diffraction, scanning electron microscopy, nitrogen physical adsorption, UV–vis diffuse reflectance spectroscopy, adsorption microcalorimetry of ammonia and carbon dioxide, temperature-programmed reduction. The interaction of NO with the catalyst surface was investigated by temperature-programmed methods. Both Cr(III) and Cr(VI) species were found on the catalysts, the content of the latter increasing along with the K loading. A bichromate phase was detected in the K-containing catalysts. Cr(VI) species underwent (incomplete) reduction under hydrogen atmosphere. The reduction extent was higher at the higher K loadings, though higher energy barriers needed to be overcome for its occurrence. All the catalysts were able to dissociate NO into atomic nitrogen and oxygen and also to convert NO into N_2O and O_2 in the temperature range 623–657 K. NO disproportionation occurred on the K-containing chromia/alumina catalysts even at relatively low temperatures (372–407 K), but not on chromia/alumina. Chromia/alumina showed an acidic as well as a basic character, the acid features being however predominant. At the lowest K content acidity appeared remarkably lowered and basicity significantly increased. Further addition of K originated a catalyst somewhat balanced in its (weak) acid–base character. At the highest K loadings the original acidic and basic features of chromia/alumina were completely lost. Such different redox and acid–base features, as well as the different interaction modes with NO, are expected to influence deeply the catalytic behaviour in 1-methylnaphthalene nitroxidation.

Keywords: Nitroxidation; 1-Methylnaphthalene; Chromia/alumina; TPR; Microcalorimetry

1. Introduction

The physical–chemical properties of chromia/alumina have been under intense scrutiny since the early 1960s [1], due to the industrial relevance of its uses as a catalyst. Among the possible applications of chromia/alumina catalysts, the nitroxidation of hydrocarbons, i.e. their one-step transformation into the corresponding nitriles by reaction with NO, has attracted attention [2–4]. Due to its particular features, nitroxidation could represent an interesting alternative to the ammoxidation reaction. Simpler catalyst formulation, safer operation and lower environmental impact act as driving forces for developing nitroxidation catalysts. Besides chromia/alumina, NiO- and PbO-based systems have also been indicated as promising candidates [2,3,5,6]. Concerning the reactant hydrocarbons, the focus has mostly been on propene [2,3,5], isobutene [2,3] and toluene [2–4,6]; propane, isobutane and xilenes have also been investigated in some detail [2,3]. Mostly relying on kinetic results [3–6], a redox mechanism has been proposed. Depending on the aliphatic or aromatic nature of the reactant hydrocarbon, an allylic or benzylic species would form on the surface of the oxidised catalyst. After loosing two more hydrogen atoms, this species would undergo attack by the atomic nitrogen originated through the dissociative adsorption of NO, while the atomic oxygen would re-oxidize the catalyst surface. The occurrence of parasite degradation of the reactant hydrocarbon has been tentatively ascribed

* Corresponding author. Fax: +39 070 675 4388.
E-mail address: ferino@unica.it (I. Ferino).

1381-1169/$ – see front matter © 2005 Elsevier B.V. All rights reserved.
doi:10.1016/j.molcata.2005.11.047

to O_2 formed from NO disproportionation into N_2O and oxygen [5]. The acidic features of the solid would also play some role, as indicated by changes in the catalyst performance when basic MgO was included in the formulation of chromia/alumina, nikel oxide/alumina and nikel oxide/silica [3]. To the best of the present authors' knowledge, just one patent [7] reports about the nitroxidation activity of alumina-supported alkali-metal oxides and no papers dealing with alkali-metal doped nitroxidation catalysts have been published so far in the open literature. Nor did studies on the reactivity of alkylpolynuclear aromatic hydrocarbons with NO appear. Doping by alkali-metal compounds is worthy of investigation. Besides modification in the catalyst acidity, perturbation of the oxidation state of the active species involved in the redox mechanism might occur as well, both these factors being expected to influence the nitroxidation activity. The use of alkylpolyaromatics as reactants for nitroxidation deserves attention. 1-Naphthonitrile, the target product of 1-methylnaphthalene (1-MN) nitroxidation, can be easily converted into 1-naphthylamide, one of the starting compounds for the production of 2-(1′-naphthyl)-5-phenyloxazole, used as a laser dye [8]. Furthermore, the understanding of 1-MN nitroxidation might be used as a reference for the conversion of 2,6-dimethylnaphthalene into the corresponding dinitrile, from which 2,6-diaminonaphthalene can be obtained. The latter is a key product for the manufacture, by reaction with adipic acid, of polymers of superior technological properties.

The present work is a part of a series devoted to the preparation, thorough characterisation and catalytic investigation of chromia/alumina, NiO-silica and NiO-alumina for the nitroxidation of 1-methylnaphthalene, for which all these oxide systems were found to be active, though to a different extent. Results concerning the preparation and characterisation of chromia/alumina catalysts are reported here. In forthcoming papers the preparation and characterisation of NiO/silica and NiO/alumina, as well as the catalytic behaviour of both chromia- and NiO-based systems, will be dealt with.

Chromia/alumina and potassium-containing chromia/alumina catalysts were prepared by the impregnation technique. The catalysts were characterised as to their chemical composition, structure, morphology and texture by atomic adsorption (AA), X-ray diffraction (XRD), scanning electron microscopy (SEM) and nitrogen physical adsorption–desorption, respectively. Information about the oxidation state of chromium was obtained by UV–vis diffuse reflectance spectroscopy (DRS). The redox features of the catalysts and the interaction of NO with the surface were investigated by temperature-programmed methods. Temperature-programmed reduction (TPR) was carried out under hydrogen flow. The nature of the species originating upon exposure of the catalyst surface to NO under temperature-programmed conditions was monitored by on-line mass-spectroscopy. Adsorption microcalorimetry, a direct and reliable quantitative technique for determining the extent and energy of adsorbate–adsorbent interactions, was used to investigate the surface acidity and basicity of the catalysts. Ammonia and carbon dioxide were chosen as probe molecules for assessing the concentration and strength-distribution of the acid and base sites, respectively.

2. Experimental

2.1. Catalyst preparation

The following catalysts were prepared: ACr10, nominally containing 10 wt.% of chromium on γ-alumina; ACr10K1, ACr10K2, ACr10K4 and ACr10K8, nominally containing also 1, 2, 4 and 8 wt.% of potassium, respectively. γ-Alumina (grain size 100–500 μm, surface area 121 $m^2\ g^{-1}$, kindly provided by Süd Chemie MT, Novara, Italy) was obtained by calcination in air of pseudoboehmite Versal 250 La Roche at 1223 K for 4 h. The support was impregnated with comparable volumes of aqueous solutions of the appropriate amounts of CrO_3 (and $K_2Cr_2O_7$ for the ACr10KX samples). The carefully stirred paste was dried overnight at 383 K and finally calcined at 973 K for 12 h. For comparison purposes a sample of crystalline chromia was prepared as in [9]. All chemicals were Carlo Erba reagent grade.

2.2. Catalyst characterisation

Chemical analysis of the total chromium content was carried out by atomic absorption (AA, Varian SpecrAA-30) on samples previously dissolved by fusion with a mixture of KNO_3 and Na_2CO_3 (1:1 by weight). A different portion of the catalyst was repeatedly treated with 1 M NaOH solution heated to incipient boiling in order to extract Cr(VI) species, and the liquid analysed by AA. The residue was then dissolved by fusion with the mixture of KNO_3 and Na_2CO_3 and analysed by AA for determining Cr(III). The potassium content was determined by AA on fresh portions of the samples after extraction with distilled hot water.

Diffuse reflectance spectra were taken in the wavelength range 200–800 nm (50,000–12,500 cm^{-1}) with a Varian CARY 5E spectrometer equipped with a PC for data acquisition and analysis and using PTFE as a reference.

Phase analysis was performed by XRD using a Philips PW 1729 diffractometer equipped with a PC for data acquisition and analysis (software APD-Philips). Scans were taken with a 2θ step of 0.01°, using Ni-filtered Cu Kα radiation. When possible, the crystallite average size was calculated by means of the Warren and Scherrer formulae [10].

Textural analyses were carried out on a Sorptomatic 1990 System (Fisons Instruments), by determining the nitrogen adsorption/desorption isotherms at 77 K. Before analysis, the samples were heated overnight under vacuum up to 473 K (heating rate = 1 K min^{-1}).

Scanning electron microscopy (SEM) images with elemental mapping of powder samples mounted on an aluminum holder were obtained on a FEI Quanta 200 microscope equipped with an EDX analyser. Semiquantitative analysis was carried out at 29 kV by using the EDAX software applying the Z.A.F. correction procedure.

TPR profiles were obtained on a TPD/R/O 1100 apparatus (ThermoQuest), under the following conditions: sample weight 0.04 g, heating rate (from 313 to 1173 K) 20 K min^{-1}, flow rate 30 $cm^3\ min^{-1}$, H_2 5% by volume in N_2; the hydrogen consumption was monitored by a thermal conductivity detector (TCD).

The same TPD/R/O 1100 apparatus (ThermoQuest), coupled with a MS detector (ProLab, Thermo Electron Corporation), was also used for investigating the interaction between NO and the catalyst surface. After reduction in H_2 (20 cm^3 min^{-1}, heating rate 30 K min^{-1} from 313 up to 713 K, held for 30 min) each sample (0.5 g) was subjected to three parallel protocols: (i) kept at 713 K under flowing H_2 while repeatedly admitting NO pulses; (ii) exposed for 30 min at 313 K to NO atmosphere (NO 10% by volume in He, flow rate 20 cm^3 min^{-1}) before starting temperature-programmed desorption (TPD experiment) under flowing He (20 cm^3 min^{-1}, heating rate 15 K min^{-1} up to 713 K, held for 60 min); (iii) exposed to NO atmosphere (NO 10% by volume in He, flow rate 20 cm^3 min^{-1}) for 30 min at 313 K and then heated (15 K min^{-1}) up to 713 K (held for 60 min) while keeping NO flowing (temperature-programmed exposure experiment, TPE). The NO, N_2O, H_2O, N_2 and O_2 MS signals were monitored during the experiments; for the temperature-programmed runs also the TCD signal was simultaneously recorded.

Tian-Calvet heat flow equipment (Setaram) was used for microcalorimetric measurements. Each sample was pre-treated overnight at 673 K under vacuum (10^{-3} Pa) before the successive introduction of the probe gas (ammonia and carbon dioxide for acidity and basicity, respectively). The equilibrium pressure relative to each adsorbed amount was measured by means of a differential pressure gauge (Datametrics). The run was stopped at a final equilibrium pressure of 133.3 Pa. The adsorption temperature was maintained at 353 K, in order to limit physisorption.

3. Results and discussion

3.1. Composition, structure, texture and morphology

Chemical composition, structural data and textural features of the chromia/alumina catalysts are summarised in Table 1. The total chromium content for the K-free catalyst (ACr10) is 9.4 wt.%. Assuming that monolayer coverage by chromium species on alumina corresponds to 0.05 wt.% CrO_3 per square metre [11] and considering the surface area value of the parent alumina (121 m^2 g^{-1}), it can be calculated that for ACr10 the total chromium amount is beyond the monolayer capacity. Most of the chromium (8.0 wt.%) is present as Cr(III), as a result of the decomposition of CrO_3 into Cr_2O_3 and O_2 during the calcination step. The XRD results for ACr10 (Table 1) show the existence, besides γ-alumina, of the α-chromia phase. Ad hoc EPR experiments on ACr10 [12] indicated that Cr(III) is also present in small clusters; traces of isolated Cr(III) and Cr(V) were detected. In spite of the high temperature of calcination, a significant amount (1.5 wt.%) of chromium remains on ACr10 in the VI valence state. In order to assess the amounts of Cr(VI) weakly and strongly bound to the support, the ACr10 sample was leached with boiling hot water for 1 h and the extract analysed. It turned out that the sample contained 0.65 wt.% Cr(VI), which represents a remarkable fraction (43%) of the hexavalent chromium species remaining on the catalyst after calcination. Quite probably, the Cr(VI) species not removed by the hot water treatment (accounting for 57% of the hexavalent chromium content) are directly anchored (grafted) on alumina by chemical bonding, a process initiated by the interaction of the precursor with OH species on the alumina surface [13]. Concerning the soluble Cr(VI) species, it can be thought that they are weakly bound because the chromium precursor either interacts with the alumina surface without formation of chemical bonds [13] or it adsorbs on surface regions where chromium precursor deposits have already accumulated [14].

The chemical composition data for the K-containing catalysts (Table 1) show that the Cr(VI) amount increases along with the potassium content, while the Cr(III) amount declines. At the highest potassium content (ACr10K8 catalyst) the Cr(III) amount is so low that the α-chromia phase is no more revealed by XRD, whereas a crystalline $K_2Cr_2O_7$ phase is present. The latter is visible, besides α-Cr_2O_3, even at the lowest K loading.

Diffuse reflectance UV–vis spectra of the investigated catalysts are shown in Fig. 1, where the spectrum of α-Cr_2O_3 is

Table 1
Characteristics of chromia/alumina and K-containing chromia/alumina catalysts

Catalyst	Composition (wt.%)				Structure		Texture	
	K	Cr_{total}	Cr(VI)	Cr(III)	Phase	D_{cryst}[a] (nm)	S_{BET}[b] (m^2 g^{-1})	V_p[c] (cm^3 g^{-1})
ACr10	–	9.4	1.5	8.0	γ-alumina α-chromia	4.2 53	94	0.35
ACr10K1	0.9	10.2	1.8	8.0	γ-alumina α-chromia $K_2Cr_2O_7$	3.7	94	0.33
Acr10K2	2.2	11.1	2.6	8.3	γ-alumina α-chromia $K_2Cr_2O_7$	4.7 40	88	0.31
Acr10K4	4.9	11.0	4.1	6.0	γ-alumina α-chromia $K_2Cr_2O_7$	4.5 66	81	0.29
Acr10K8	6.0	11.6	8.2	2.8	γ-alumina $K_2Cr_2O_7$	4.5	51	0.21

[a] Crystallite size.
[b] Surface area.
[c] Pore volume.

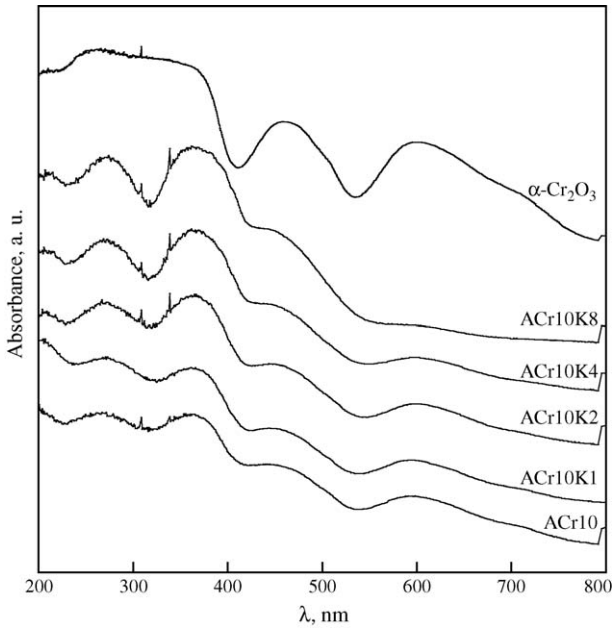

Fig. 1. Diffuse reflectance UV–vis spectra of the investigated chromia/alumina catalysts. The spectrum for α-chromia is also shown.

also reported for reference. The UV–vis region is diagnostic for the presence of Cr(VI) in tetrahedral coordination and Cr(III) in octahedral symmetry. Four absorption bands can be evidenced from the figure: two charge transfer transitions $O \rightarrow Cr$ typical of Cr(VI) at $\lambda \sim 278$ nm and 370 nm and two bands due to d–d transitions of Cr(III) at $\lambda \sim 463$ nm ($A_{2g} \rightarrow T_{1g}$) and 600 nm ($A_{2g} \rightarrow T_{2g}$). An increase in Cr(VI) concentration with the K-content is manifest from the increasing values of the peak intensity at 278 and 370 nm, thus confirming the results of chemical analyses (Table 1). The pronounced increase in the concentration of the hexavalent chromium species observed along with the increase in potassium loadings is consistent with the progressive development of the bichromate phase.

The textural data (Table 1) show a decreasing trend in both surface area and pore volume as the potassium content increases, hence suggesting progressive pore plugging. For all the catalysts the adsorption–desorption isotherm appeared of type IV [15] with an hysteresis loop of type H1, which is indicative of mesoporous materials with open-ended cylindrical pores [16]. A monomodal distribution of pore diameter, centred around 129–134 nm, was observed (Dollimore–Heal method [17]). *t*-Plot analysis (Lecloux *n*-method [18]) did not reveal the presence of micropores.

SEM images of selected catalysts are shown in Figs. 2 and 3. The surface morphology of the ACr10 sample is visible in Fig. 2a, taken in the large field detector (LFD) mode; relatively large particles are in evidence on a more uniform background. The same shot taken in the solid state detector (SSD) mode (Fig. 2b) and EDX analysis data (not shown) indicate that these are α-chromia particles. At higher magnification (Fig. 2c) the latter appear as agglomerates of smaller crystallites, whose dimensions are consistent with those obtained by XRD. Shots of the ACr10K8 surface in the LFD and SSD modes (Fig. 3a and

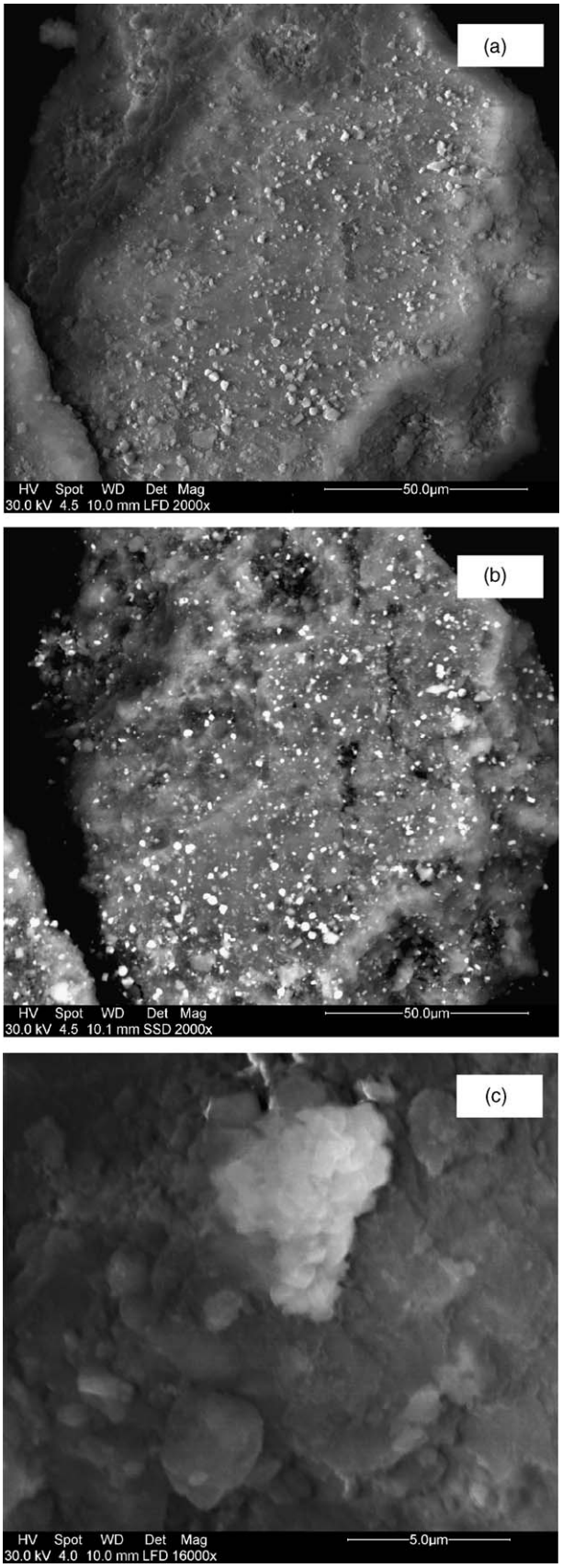

Fig. 2. SEM images of the chromia/alumina (ACr10) catalyst: (a) LFD mode, 2000×; (b) SSD mode, 2000×; (c) LFD mode, 16,000×.

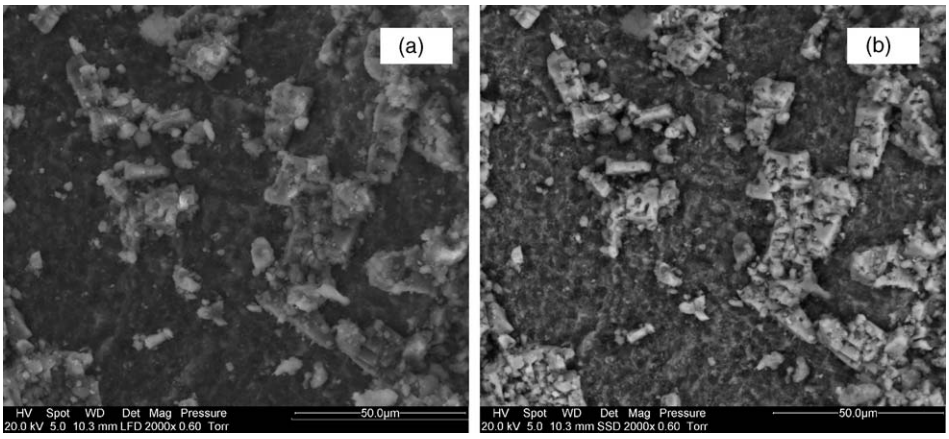

Fig. 3. SEM images of a K-containing (ACr10K8) catalyst: (a) LFD mode, 2000×; (b) SSD mode, 2000×.

b, respectively) reveal the presence of relatively large $K_2Cr_2O_7$ crystals, thus confirming the XRD findings.

3.2. Redox features

The ability of the active species of the catalyst to shift from higher to lower valence states upon exposure to the reactant hydrocarbon is of key importance for the catalytic activity. The behaviour of the different catalysts under reducing atmosphere in temperature-programmed runs is hence worthy of investigation.

The temperature-programmed reduction profile of ACr10 is presented in Fig. 4, where the TPR profiles for the parent γ-alumina and a pure α-chromia sample are also reported for comparison. As expected, no hydrogen consumption occurs for γ-alumina. For the pure chromia sample a symmetric peak, followed by two broad merging peaks of quite low area, is observed.

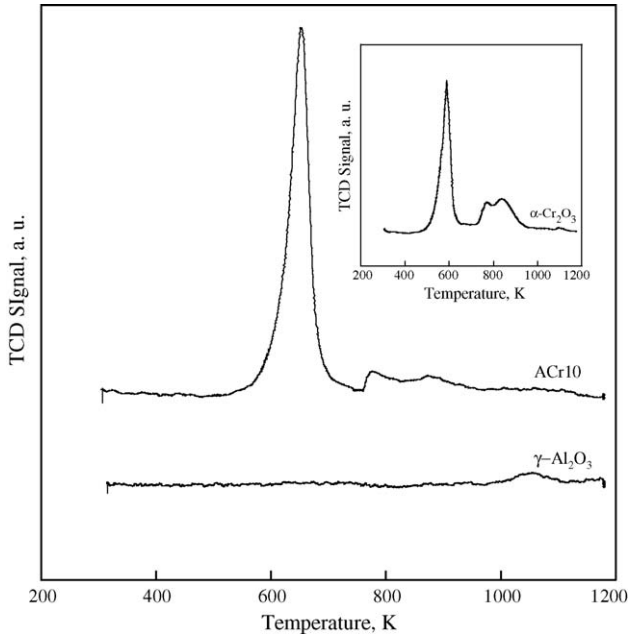

Fig. 4. Temperature-programmed reduction profiles for the chromia/alumina (ACr10) catalyst, the parent γ-alumina and (inset) a α-chromia sample.

Such a result has been already reported by other authors [19], who ascribed the main peak to the reduction of Cr(VI) to Cr(III) species. These same authors also suggested that the broad, merging peaks could stem either from bulk reduction of Cr(III) to lower oxidation states or from activated hydrogen adsorption, evidence for which had been previously reported [20,21]. The TPR profile for ACr10 is quite similar to that of pure chromia. Accordingly, the symmetric peak visible for ACr10 (maximum at 653 K) can be associated with the transformation of Cr(VI) species into Cr(III).

To find a clue to the origin of the very low-area broad peaks in the reduction profile of ACr10 (i.e. whether or not they are related to bulk reduction of Cr(III)) further runs have been carried out. Two other chromia/alumina samples of the same composition as ACr10 were prepared, the only difference being in the temperature of the calcination step: 973 K for ACr10, 1073 and 1173 K for the two other samples, henceforth named ACr10-1073 and ACr10-1173, respectively. Chemical analyses gave a residual Cr(VI) content of 1.30 wt.% for ACr10-1073 and 0.60 wt.% for ACr10-1173, i.e. lower than that for ACr10 (1.50 wt.%), due the higher calcination temperature of the former samples. The TPR profiles of ACr10-1073 and ACr10-1173 were obtained; they are compared with that for ACr10 in Fig. 5. As expected, the higher the calcination temperature the lower the main peak area, the latter being related to the residual Cr(VI) content. The two broad, ill-defined peaks present in the TPR spectrum of ACr10 are no more visible for ACr10-1073 and ACr10-1173, in spite of the increased Cr(III) content resulting from the higher calcination temperature. Accordingly, the reduction of Cr(III) to lower valence states cannot be invoked to explain the ill-defined TPR signal in ACr10. Anyway, the contribution of the low-area broad peaks to the total hydrogen consumption during the reduction of ACr10 is extremely low and has hence been disregarded. By considering that 3 mol of hydrogen are needed for the transformation of 2 mol of Cr(VI) into Cr(III), the reduction extent, α, can be calculated from the Cr(VI) content. The resulting α value (45%) indicates incomplete reduction of Cr(VI) species during the TPR run. The close agreement between this value and the fraction of water-soluble Cr(VI) (43%) suggests that only the hexavalent

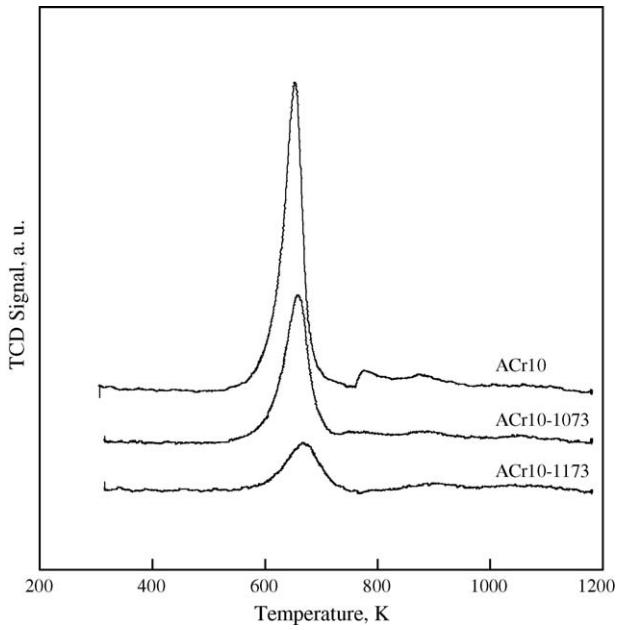

Fig. 5. Temperature-programmed reduction of chromia/alumina after calcining at 773, 1073 and 1173 K (ACr10, ACr10-1073 and ACr10-1173 samples, respectively).

chromium species weakly bound to the support undergo reduction.

The TPR results for the K-containing chromia/alumina catalysts are shown in Fig. 6, where the reduction profile for ACr10 is also reported. Remarkable differences in the reduction behaviour of the samples are evident from both the shape and maximum temperature, T_{max}, of the peaks. The latter are listed in Table 2, together with the calculated reduction extent of Cr(VI). The

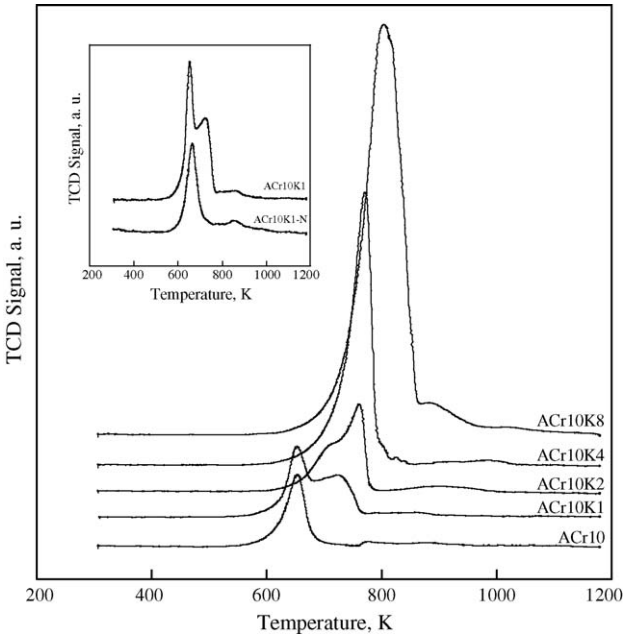

Fig. 6. Temperature-programmed reduction of the K-containing chromia/alumina catalysts. Chromia/alumina (ACr10) is also shown. ACr10K1N, obtained by calcining in nitrogen instead of air, is compared with ACr10K1 in the inset.

Table 2
Temperature-programmed reduction results for chromia/alumina and K-containing chromia/alumina catalysts

Catalyst	T_{max}[a] (K)	α[b] (mol%)
ACr10	380	45
ACr10K1	379; 449	55
ACr10K2	488	42
ACr10K4	498	55
ACr10K8	531	69

[a] Maximum temperature of H_2 consumption.
[b] Reduction extent.

reduction of ACr10K1 originates two peaks, a clearly defined one (T_{max} = 652 K) and an enlarged one (T_{max} = 722 K). It seems that, besides the Cr(VI) species originally present on chromia/alumina, a new Cr(VI) species, which undergoes reduction at higher temperature, is formed upon the addition of a small amount (1 wt.%) of K. The reduction profile of ACr10K2 shows a peak with T_{max} = 761 K, with a shoulder appearing before the maximum. The TPR spectrum for ACr10K4 shows an asymmetric (heading) peak with T_{max} = 771 K. The shoulder in ACr10K2 and the heading in ACr10K4 reveal also for these samples the presence of the two different Cr(VI) species, with the tendency for the one reducing at higher temperature to become by far predominant. One large peak, further shifted at higher temperatures (T_{max} = 804 K), appears in the TPR spectrum of ACr10K8; accordingly, hexavalent chromium of only one kind would be present on this sample.

In the inset of Fig. 6 the TPR profile of ACr10K1 is compared with that for another sample, named ACr10K1N. The latter was obtained by the same procedure followed for ACr10K1, the only difference being that nitrogen instead of air was used for ACr10K1N during the heating step at 973 K. Comparison of their TPR profiles shows the lack of the second peak in ACr10K1N, i.e. the high-temperature reducing Cr(VI) species is lacking in this sample. At variance with ACr10K1, ACr10K1N did not show in its XRD pattern the presence of the bichromate phase. Accordingly, it could be suggested that the second peak in ACr10K1 (T_{max} = 722 K) is originated by Cr(VI) present as bichromate. Also the peaks at 761, 771 and 804 K in ACr10K2, ACr10K4 and ACr10K8, respectively, would be related to the reduction of bichromate Cr(VI) species, whose amount grows with the K loading. The shoulder in ACr10K2 and the heading in ACr10K4 profiles would stem from residual Cr(VI) present as chromium oxide, which progressively declines along the series ACr10 > ACr10K1 > ACr10K2 > ACr10K4. At the highest K loading (ACr10K8) Cr(VI) is present only as bichromate, whose reduction gives the large peak with T_{max} = 804 K.

It is worthy of note that the reduction of Cr(VI) is largely incomplete (α = 42–55%) for K loadings up to 4 wt.%. For ACr10K8 the reduction extent is markedly higher (α = 69%). On the one hand, the reduction seems to go further towards completeness at the higher K loadings, while, on the other, higher energy barriers need to be overcome for the establishing of the reduction process. It seems that, as the organised bichromate phase develops as the major component, the Cr(VI) species interact so weakly with the alumina support that only a minor fraction

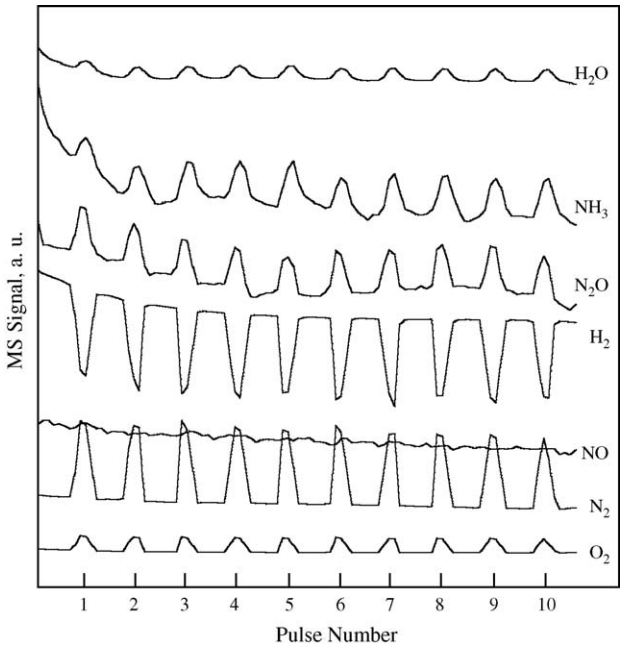

Fig. 7. MS signals recorded upon admission of NO pulses onto a K-containing chromia/alumina (ACr10K8) catalyst kept at 713 K under flowing hydrogen.

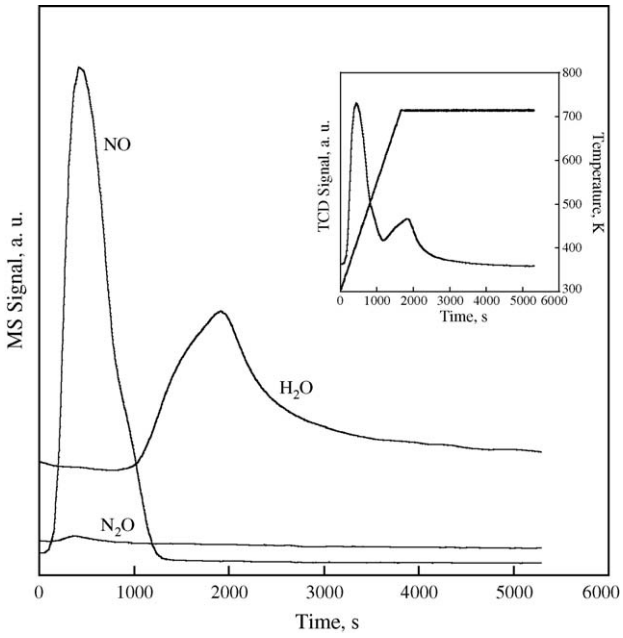

Fig. 8. TCD (inset) and MS signals recorded during temperature-programmed desorption (TPD) under He atmosphere of formerly adsorbed NO on chromia/alumina (ACr10) catalyst.

of them remains unreduced; the reduction of the bichromate phase, however, requires high activation energy.

3.3. NO interaction with the catalyst surface

The interaction between NO and the catalyst surface was investigated on ACr10, ACr10K1, ACr10K2 and ACr10K8. All of the catalysts appeared able to dissociate NO into atomic nitrogen and oxygen. Evidence from this was obtained from isothermal runs at 713 K, in which NO pulses were admitted on the catalyst simultaneously exposed to flowing hydrogen. The case of ACr10K8 is presented in Fig. 7 as an example, the behaviour of the other catalysts being quite similar. It is evident from the MS signals that consumption of the NO pulse (and H_2) occurs simultaneously with NH_3 (and H_2O) formation, which indicates that atomic nitrogen is formed from NO on the catalyst surface. Both N_2O and O_2 formation is also visible in correspondence with NO consumption, which suggests the occurrence of disproportionation to some extent. This point is worthy of further investigation because of the possible involvement of O_2 generated through this way in the reactant degradation during the nitroxidation reaction, as previously mentioned in Section 1.

Accordingly, temperature-programmed desorption experiments (TPD) under He atmosphere of formerly adsorbed NO and temperature-programmed exposure (TPE) to NO atmosphere were carried out on the catalysts. The results for ACr10 are presented in Figs. 8 and 9, respectively. The TCD signal recorded for ACr10 during the TPD run (Fig. 8, inset) shows two peaks. The one at 406 K can be ascribed to NO desorption (cf. the MS signal for NO in the same Fig. 8), accompanied by traces of N_2O (cf. the very weak MS signal for N_2O in the same Fig. 8). The peak in the isothermal region at 713 K seems related to water desorption (cf. the MS signal for H_2O in the same Fig. 8), resulting from dehydroxylation of the catalyst surface. The TCD signal recorded during the TPE experiment (Fig. 9, inset) stems from diverse contributions, which can be identified on the basis of the MS signals (also shown in Fig. 9). The evolution of the NO signal with temperature reveals that the gas stream becomes initially enriched in this component (which is consistent with a release of NO from the sample) and then the gas stream becomes impoverished in NO until the original content is attained again (as if NO consumption had occurred). Simultaneously with NO

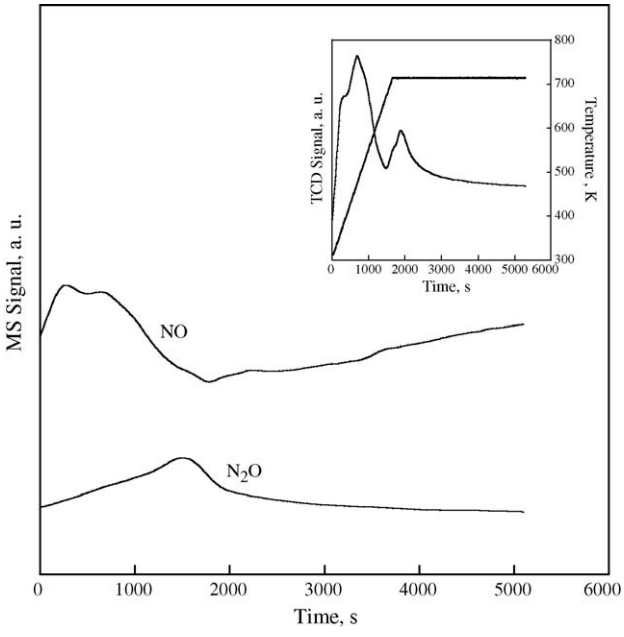

Fig. 9. TCD (inset) and MS signals recorded during temperature-programmed exposure (TPE) to NO atmosphere of chromia/alumina (ACr10) catalyst.

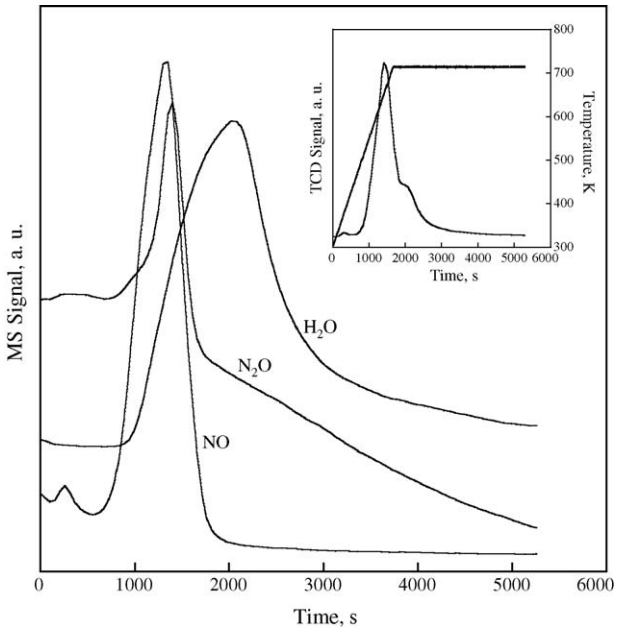

Fig. 10. TCD (inset) and MS signals recorded during temperature-programmed desorption (TPD) under He atmosphere of formerly adsorbed NO on K-containing chromia/alumina (ACr10K8) catalyst.

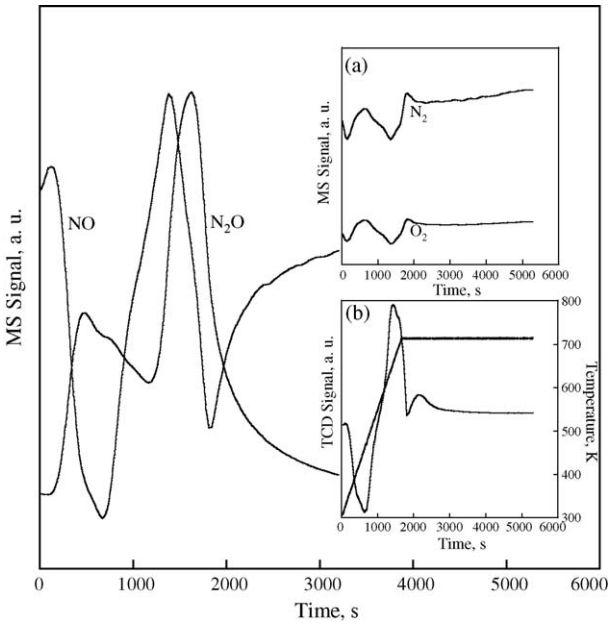

Fig. 11. TCD (inset) and MS signals recorded during temperature-programmed exposure (TPE) to NO atmosphere of K-containing chromia/alumina (ACr10K8) catalyst.

consumption, a peak appears in the MS signal for N_2O. Accordingly, the following sequence of events can be envisaged: (i) desorption of NO (formerly adsorbed during the isothermal step at 313 K) sets in as a consequence of the increasing temperature; (ii) further increase in temperature causes NO transformation, catalysed by the solid, into N_2O and O_2; (iii) water release occurs at higher temperatures, due to dehydroxylation of the catalyst surface.

Results for ACr10K8 catalyst are presented in Fig. 10 (TPD run) and 11 (TPE run). The TCD signal (Fig. 10, inset) peaks at 373 and 653 K, as well as in the isothermal region at 713 K. Both the first and second (remarkably larger) peak seem originated by NO desorption (cf. the MS signal for NO in the same Fig. 10). Simultaneous evolution of N_2O can be observed, as indicated by the MS signal for this species. The third peak corresponds to water released by surface dehydroxilation (cf. the MS signal for H_2O in the same Fig. 10). Heating the sample under NO atmosphere gives the MS signals shown in Fig. 11, which reveal NO consumption in two different temperature regions, associated with N_2O formation. Simultaneous O_2 and N_2 formation can be also observed (inset (a) in Fig. 11), particularly in correspondence with the low-temperature NO consumption. It seems that the solid catalyses the transformation of NO into N_2O and O_2, as well as, to some extent, the further conversion of N_2O into N_2 and O_2. Accordingly, the TCD profile (inset (b) in Fig. 11) is rather complex.

The TPD and TPE results for ACr10K1 are presented in Figs. 12 and 13, respectively; those for ACr10K2 are shown in Figs. 14 and 15. While ACr10K1 still exhibits some of the original features of ACr10, these are completely lost on ACr10K2. The features of the latter are rather similar to those of ACr10K8, though less pronounced.

The main issues of the TPE runs can be summarised as follows. NO conversion into N_2O (and O_2) occurs over all the catalysts in a narrow temperature range (623–657 K), to an increasing extent along the series ACr10 < ACR10K1 < ACr10K2 < ACr10K8. The K-containing samples (ACr10K1, ACr10K2 and ACr10K8) catalyse NO conversion into O_2 and N_2O even at relatively low temperatures (372–407 K). On ACr10 no significant consumption of NO from the gas stream occurs at

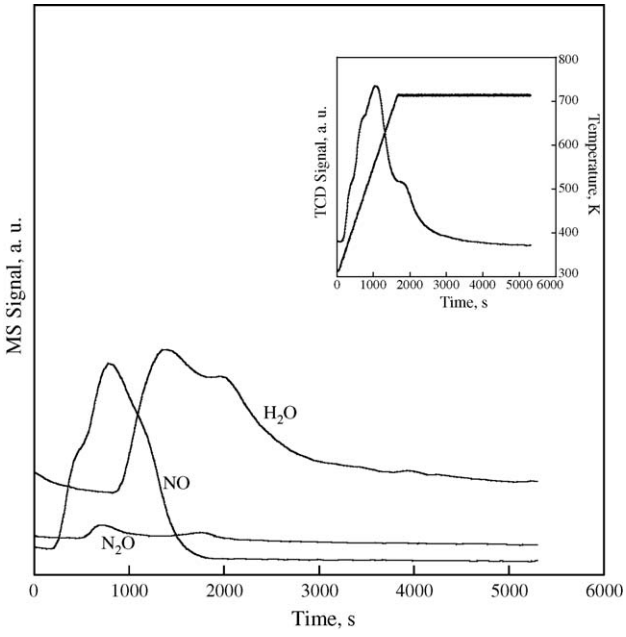

Fig. 12. TCD (inset) and MS signals recorded during temperature-programmed desorption (TPD) under He atmosphere of formerly adsorbed NO on K-containing chromia/alumina (ACr10K1) catalyst.

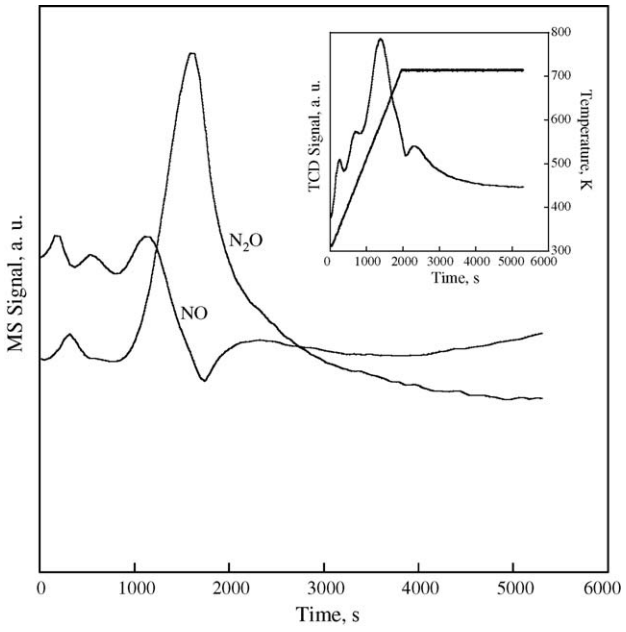

Fig. 13. TCD (inset) and MS signals recorded during temperature-programmed exposure (TPE) to NO atmosphere of K-containing chromia/alumina (ACr10K1) catalyst.

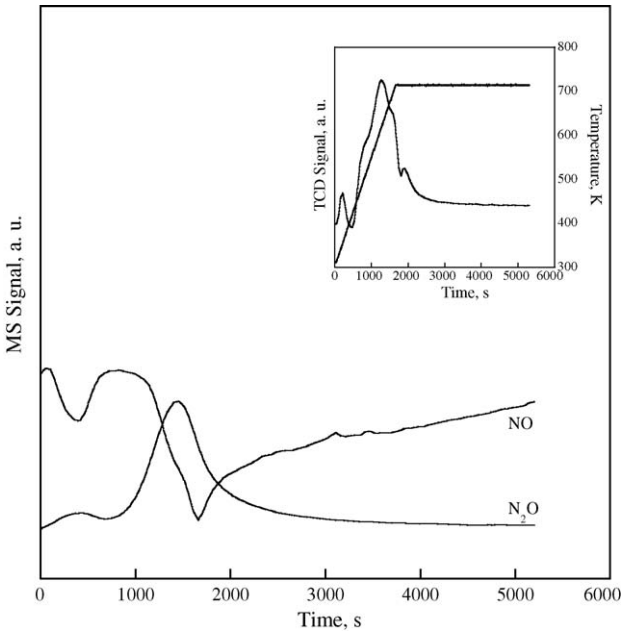

Fig. 15. TCD (inset) and MS signals recorded during temperature-programmed exposure (TPE) to NO atmosphere of K-containing chromia/alumina (ACr10K2) catalyst.

such low temperatures, only traces of N_2O being visible; instead, NO (formerly adsorbed during the isothermal step at 313 K) is released from the surface.

3.4. Surface acidity and basicity

The results of the microcalorimetric runs aimed at determining the acid features of the catalysts, are reported in Fig. 16, where the differential heat of adsorption, Q_{diff}, is plotted versus the ammonia uptake, n_A, for the various samples, including the parent γ-alumina and the pure α-chromia. For γ-alumina the Q_{diff} value is initially rather high (ca. 245 kJ mol^{-1}), dramatically drops after the first ammonia dose and then continues to decrease, though with a smoother trend, as the coverage increases (approaching a final value of ca. 50 kJ mol^{-1}). Such a continuous heterogeneity in the strength of the ammonia adsorbing (i.e. acid) sites, occurring over a wide range of differential heat of adsorption, stems from both "chemical" and "crystallographic" heterogeneity of the surface. The first is originated

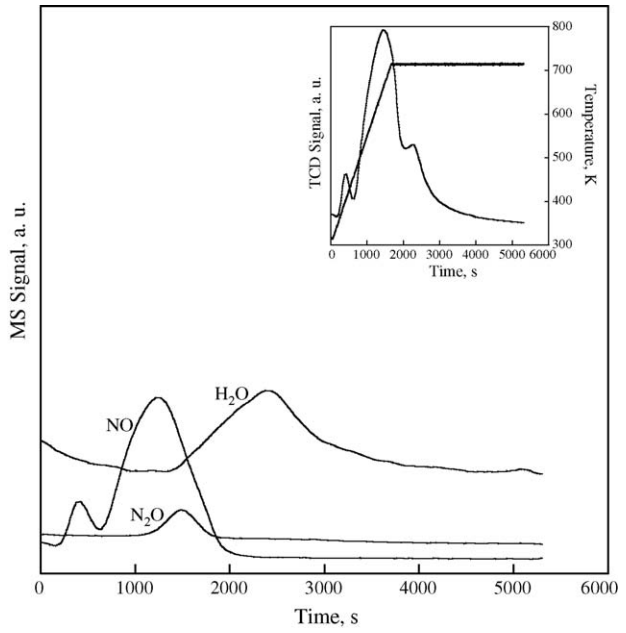

Fig. 14. TCD (inset) and MS signals recorded during temperature-programmed desorption (TPD) under He atmosphere of formerly adsorbed NO on K-containing chromia/alumina (ACr10K2) catalyst.

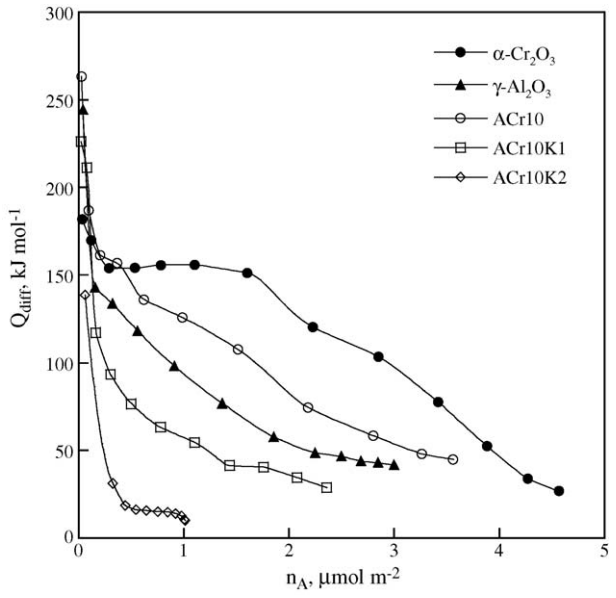

Fig. 16. Differential heat of adsorption, Q_{diff}, as a function of ammonia uptake, n_A, for γ-Al_2O_3, α-Cr_2O_3, chromia/alumina (ACr10) and K-containing chromia/alumina (ACr10K1 and ACr10K2) catalysts.

by the different nature of the acid sites, namely, coordinatively unsaturated (cus) aluminium ions and OH groups of the hydroxylated surface. Crystallographic heterogeneity is related to the location of a given adsorbing site on faces, steps or kinks of the crystallites. After a short decrease, the Q_{diff} versus n_A profile for α-chromia shows a plateau at ca. 152 kJ mol^{-1}, accounting for about one third of the total ammonia uptake, followed by a continuous decrease as the coverage increases further. This indicates the presence of a relatively large set of acid sites homogeneous as to their strength, quite probably Cr_{cus}^{3+} ions in well-defined α-Cr_2O_3 crystals. The decreasing trend is reasonably related to the chemical heterogeneity stemming from the presence of Cr_{cus}^{6+} ions, as well as to crystallographic heterogeneity of both Cr_{cus}^{3+} and Cr_{cus}^{6+}. Some contribution from acid OH groups cannot be excluded. However it should be quite limited, due to the very low tendency of chromia to adsorb water dissociatively [22].

The acid features of ACr10 appear enhanced in comparison with those of the parent alumina, due to the presence of the deposited chromia. A certain character of both γ-Al_2O_3 and α-Cr_2O_3 seems to be somewhat retained in the chromia/alumina sample. The rather high Q_{diff} value (ca. 265 kJ mol^{-1}) resembles that of γ-alumina, a plateau is visible at ca. 155 kJ mol^{-1}, i.e. similar to that of α-chromia, though rather shorter, and the continuously decreasing part of the Q_{diff} versus n_A profile lies between those for the parent alumina and the pure α-chromia. A variety of cus ions able to interact with ammonia are present on the surface of ACr10. These include Cr_{cus}^{3+} and Cr_{cus}^{6+}, as well as Al_{cus}^{3+}, if the alumina surface is not completely covered by chromia; OH groups might as well contribute to the surface acidity, if the surface is hydroxylated to some extent. Besides chemical heterogeneity, crystallographic heterogeneity adds complexity to the acid strength distribution of the catalyst surface. A detailed discussion relating each of these contributions to the surface acidity with the specific trend of Q_{diff} versus n_A cannot hence be attempted.

However the influence of potassium on the acidity of the chromia/alumina is clearly visible in Fig. 16. The Q_{diff} versus n_A curve for ACr10K1 lies below that for ACr10; furthermore, the total ammonia uptake is significantly lower in the case of ACr10K1. This indicates that both the concentration and strength of the acid sites have decreased, due to presence of potassium. An increase in the latter from 1 to 2 wt.% shifts further the Q_{diff} versus n_A curve towards lower Q_{diff} values. It is also worthy of note that for ACr10K2 the differential heat of adsorption suddenly drops from ca. 140 to 20 kJ mol^{-1}, and then does not change significantly as n_A increases. Such low values of Q_{diff}, identical with the liquefaction heat of NH_3 (20.2 kJ mol^{-1} at 353 K, calculated by the Watson relation [23]) and extending over a large part of the calorimetric curve, indicate that most of the ammonia adsorbed on ACr10K2 is physically held on the surface by non-specific interactions. Only the first part of the curve is hence originated by the adsorption on the acid sites, whose concentration is quite low (ca. 0.4 μmol m^{-2}) in comparison with ACr10K1 and ACr10 (ca. 2.4 and 3.6 μmol m^{-2}, respectively). No ammonia uptake was observed on ACr10K4 and ACr10K8; accordingly, these samples can be regarded as non-acidic.

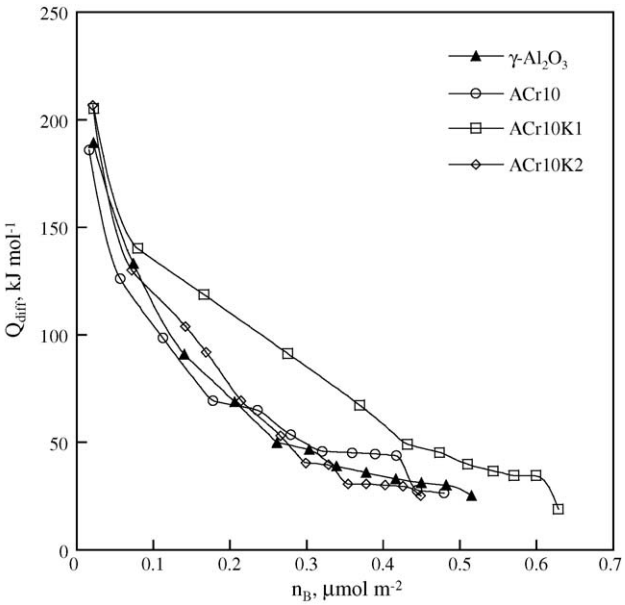

Fig. 17. Differential heat of adsorption, Q_{diff}, as a function of carbon dioxide uptake, n_B, for γ-Al_2O_3, chromia/alumina (ACr10) and K-containing chromia/alumina (ACr10K1 and ACr10K2) catalysts.

The results concerning carbon dioxide adsorption on γ-Al_2O_3, ACr10, ACr10K1 and ACr10K2 are shown in Fig. 17, where the differential heat of adsorption, Q_{diff}, is plotted versus the CO_2 uptake, n_B. No adsorption of carbon dioxide was observed on α-Cr_2O_3, ACr10K4 and ACr10K8. The Q_{diff} value for ACr10 rapidly drops from ca. 185 to 75 kJ mol^{-1} as coverage increases up to ca. 0.2 μmol m^{-2}, indicating continuous heterogeneity of the basic sites. Reasonably, these CO_2 adsorbing sites are oxygen ions, differing as to their chemical and/or crystallographic environment; basic hydroxyls might be present as well. Increasing in coverage up to ca. 0.5 μmol m^{-2} is accompanied by further decrease in Q_{diff}, until a value of ca. 25 kJ mol^{-1} is attained. The somewhat stepwise character of the curve in this region suggests the presence of sets of sites homogeneous as to their strength, though no details about their nature can be given. Comparison of the ACr10 and γ-Al_2O_3 profiles shows no significant change in the basic character of the parent alumina upon chromia deposition, which is in agreement with the observed lack of basicity for α-Cr_2O_3.

The basic features of the chromia/alumina are significantly perturbed upon addition of 1 wt.% K. The Q_{diff} versus n_B profile for ACr10K1 lies above that for ACr10 and extends over a larger n_B range, i.e. both the concentration and strength of the basic sites appear enhanced. Interestingly, such an increase in basicity does not occur upon addition of 2 wt.% of K to chromia/alumina. The Q_{diff} versus n_B profile for ACr10K2 lies slightly above that for ACr10 for $n_B <$ ca. 0.2 μmol m^{-2}, which suggests that such an uptake results from the interaction of carbon dioxide with slightly stronger sites in the case of ACr10K2. On the contrary, for $n_B >$ ca. 0.2 μmol m^{-2} CO_2 adsorption involves the interaction with slightly weaker sites in the case of ACr10K2: the Q_{diff} versus n_B curve for this catalyst is now below that for ACr10 and

approaches the limit for physical adsorption (at 353 K the liquefaction heat of CO_2, calculated by the Watson relation [23], is 13.7 kJ mol^{-1}). Increasing further the amount of K is even detrimental for the basic features of the chromia/alumina catalysts: adsorption of carbon dioxide did not occur at all on ACr10K4 and ACr10K8 catalysts.

In summary, the outcome of the microcalorimetric experiments seems the following: (i) chromia/alumina has acidic as well as basic character, though the acid features prevail (in terms of both concentration and strength); (ii) a small amount (1 wt.%) of K remarkably decreases acidity and significantly increases basicity; (iii) further addition of K (up to 2 wt.%) strongly decreases acidity but also lowers basicity, the catalyst appearing now somewhat balanced in its (weak) acid–base character; (iv) in the presence of high (4 and 8 wt.%) K loadings, both the original acidic and basic features of chromia/alumina are completely lost.

4. Conclusions

Based on the results of the present work, the following conclusions can be drawn. The redox features, the NO-surface interactions and the acid–base properties of chromia/alumina can be modified by introducing potassium in the catalyst formulation. By suitably dosing the potassium amount, new Cr(VI) species can be generated, and the extent of catalyst reduction can be enhanced, though higher reduction temperatures are needed. It is also possible to induce in the catalyst low-temperature activity for the conversion of NO into N_2O and O_2. Modulation of the acid–base features of the catalyst can be also achieved. Fall-out on the activity of the catalysts for the nitroxidation of 1-methylnaphthalene is expected.

References

[1] C.P. Poole, D.S. MacIver, Adv. Catal. 17 (1967) 223.
[2] G.M. Pajonk, Appl. Catal. A: Gen. 72 (1991) 217, and literature therein.
[3] G.M. Pajonk, J. Chim. Phys. 88 (1991) 547, and literature therein.
[4] M.K. Younes, M.K. Ghorbel, Appl. Catal. A: Gen. 197 (2000) 269.
[5] G.M. Pajonk, T. Manzalji, Catal. Lett. 21 (1993) 361.
[6] R.P. Prasad, A. Garg, S. Matthews, J. Chem. Eng. 72 (1994) 164.
[7] H. Satou, K. Hirose (Sumitomo Chemical Co.), JP. Pat. 60 028 939 (1985).
[8] H.H. Szmant, Organic Building Blocks of the Chemical Industry, Wiley, New York, 1989.
[9] S. De Rossi, G. Ferraris, S. Fremiotti, V. Indovina, A. Cimino, Appl. Catal. A: Gen. 106 (1993) 125.
[10] H.P. Klug, L.E. Alexander, X-Ray Diffraction Procedures, 3rd ed., Wiley, New York, 1962.
[11] M.A. Vuurman, F.D. Hardcastle, I.E. Wachs, J. Mol. Catal. 84 (1993) 193.
[12] D. Cordischi, Private communication.
[13] F. Cavani, M. Koutyrev, F. Trifirò, A. Bartolini, D. Ghiseletti, R. Iezzi, A. Santucci, G. Del Piero, J. Catal. 158 (1996) 236, and literature therein.
[14] L.R. Mentasty, O.F. Gorriz, L.E. Cadus, Ind. Eng. Chem. Res. 38 (1999) 396.
[15] IUPAC Reporting physorption data for gas/solid systems, Pure Appl. Chem. 57 (1985) 603.
[16] F. Rouquerol, J. Rouquerol, K. Singh, Adsorption by Powders & Porous Solids, Academic Press, London, 1999.
[17] D. Dollimore, G.R. Heal, J. Appl. Chem. 14 (1964) 109.
[18] A.J. Lecloux, in: J.R. Anderson, M. Boudart (Eds.), Catalysis, Science and Technology, vol.2, Springer-Verlag, Berlin, 1981, p. 187.
[19] B. Grzybowska, J. Słoczński, R. Grabowski, K. Wcisło, A. Kozłowska, J. Stoch, J. Zieliński, J. Catal. 178 (1998) 687, and literature therein.
[20] S.W. Weller, S.E. Voltz, J. Am. Chem. Soc. 76 (1954) 4695.
[21] S.E. Voltz, S.W. Weller, J. Am. Chem. Soc. 76 (1954) 4701.
[22] A. Zecchina, S. Coluccia, E. Guglielminotti, G. Ghiotti, J. Phys. Chem. 75 (1971) 2774.
[23] R.C. Reid, J.M. Prausnitz, B.E. Poling, The Properties of Gases and Liquids, 4th ed., McGraw-Hill, New York, 1987.